Current Applied Physics 18 (2018) 90–95

Contents lists available at ScienceDirect

Current Applied Physics

journal homepage: www.elsevier.com/locate/cap

Electronic transport properties of graphene/Al_2O_3 (0001) interface

M.S. Gusmão [a], Angsula Ghosh [a, b], H.O. Frota [a, *]

[a] Department of Physics, Federal University of Amazonas, 69077-000, Manaus, AM, Brazil
[b] São Paulo State University(Unesp), Institute for Theoretical Physics (IFT), São Paulo, SP, Brazil

ARTICLE INFO

Article history:
Received 5 June 2017
Received in revised form
3 October 2017
Accepted 10 October 2017
Available online 14 October 2017

Keywords:
Graphene
Alumina
DFT
Transport properties

ABSTRACT

The electronic structure and transport properties of a single layer of graphene (Gr) on α-Al_2O_3 surface are studied using the density functional theory (DFT). We present three models that take into account the atom at the termination of the alumina surface: a) Al atoms, with the center of the Gr hexagon directly over an Al atom; b) Al atoms, with a carbon directly positioned above an Al atom; c) oxygen atoms. Two processes of geometric optimization were used: (**i**) All the atoms of the supercell were allowed to move in accordance with the BFGS quasi-Newton algorithm; (**ii**) The atoms of the three topmost layers of the α-Al_2O_3 (0001) slab, including the C atoms, were allowed to move, whereas the atoms of the remaining layers were frozen in their respective atomic bulk positions. The first two models preserve qualitatively the electronic structure of the pristine Gr using the geometric optimization process (**i**) whereas, in the third model this structure was lost due to a significant charge transfer between the carbon and oxygen atoms irrespective of the optimization procedure. However, models (a) and (b) with the optimization (ii) reveal a p-type semiconducting behavior.

1. Introduction

The Pioneering works on graphene (Gr) by Andre Geim and Kostya Novoselov [1–3] led to an increasing interest in the scientific community to study this new material. The works were mainly motivated by its exceptional electronic properties, such as its non-massive fermion behavior at low excitation energies and high mechanical strength (200 times stronger than steel) and potential applications these properties offer for the future. The discovery brought new perspectives to nanotechnology development, with graphene being a probable substitute to the current electronics based on silicon. Nowadays, the major challenge of the scientists and the engineers is to obtain a low cost scalable production of single layer graphene with an aim to consolidate its application in nanoelectronics, energy technology, composite materials, sensors, among other fields of interest [4,5].

The increasing interest in nanoscience and nanotechnology has also induced a great enthusiasm in the study of α-Al_2O_3 (0001) crystal [6–10]. The hexagonal symmetry, a high dielectric constant have evoked its use in electronic devices. Recently, a systematic study of α-Al_2O_3 (0001) crystal [11] has compared their results using DFT (Density Functional Theory) calculations with those of the experimental measurements obtained from XPS (X-ray photoelectron spectroscopy) and UPS (ultraviolet photoelectron spectroscopy) spectra. A band gap of 6.26 eV between the conduction and the valence bands, and an ionic gap of 8.9 eV (where the ionic gap refers to the gap between the upper and lower valence bands), were calculated utilizing a unit cell of 30 atoms. However, the calculated band gap of 6.26 eV is much smaller than 8.8 eV obtained from the electron energy spectrum and 8.7 eV obtained from optical spectra [12]. This discrepancy between the theoretical and the experimental results can be attributed to the underestimation of bandgap width of solids in DFT methods.

Recent experimental studies and theoretical models have been used to understand the electronic properties of contact between Gr and the α-Al_2O_3 (0001) surface [13–22]. This is mainly due to the small lattice mismatch of the α-Al_2O_3 (0001) surface with respect to graphene. The above lattice similarity that minimizes the elastic energy in the interface makes it suitable for electronic applications. The dual-gated graphene field-effect transistor with Al_2O_3 as top-gate dielectric [13] observed mobility values above 8000 $cm^2/V/s$ which is a very promising result. It is important to remember that the mobility of charge carriers in free graphene lies between 10000 and 15000 $cm^2/V/s$ [18]. Lately, a single layer graphene transistor on 72 nm α-Al_2O_3 film exhibited a seven times higher interelectrode conductivity than that on a 300 nm SiO_2 film, due to the smaller

* Corresponding author.
E-mail address: hfrota@ufam.edu.br (H.O. Frota).

https://doi.org/10.1016/j.cap.2017.10.008
1567-1739/

dielectric thickness and higher dielectric constant of α-Al_2O_3 [14]. Of late, the DFT study [21] of the band structure of (0001) α-Al_2O_3 surface and the interface of single layer graphene with α-Al_2O_3, for different arrangements of graphene on (0001) α-Al_2O_3 surface demonstrated Gr adsorption on the surface terminated with Al atoms. More recently, the low-cost synthesis of Gr/α-Al_2O_3 nanosheet interfaces using bimetallic alloys has been of utmost importance for its application in electronic devices [20]. The samples grown by chemical vapor deposition and selective oxidization were characterized by angle resolved photoemission (ARPES), XPS and low energy electron diffraction (LEED). The ARPES spectrum confirmed that the Dirac cone in the vicinity of the Fermi energy is fully restored, indicating the formation of a thick oxide layer decoupled from the metallic alloy.

In this work we used DFT to calculate some transport properties of a single layer graphene on α-Al_2O_3 (0001) surface, such as electrical conductivity and electronic thermal conductivity. The calculations were performed using the Quantum Espresso [23] and BoltzWann [24] packages.

2. Computational methods and models

All the numerical calculations were performed using the density functional theory (DFT) as implemented in Quantum Espresso package [25]. The Perdew, Burke, and Ernzerhof (PBE) [26] functional based on the generalized gradient approximation (GGA) was used to describe the exchange-correlation energy. The constraint-free geometry optimization was obtained using the BFGS quasi-Newton algorithm, with the convergence thresholds set at 10^{-3} eV/Å for force and 10^{-4} eV for energy. We introduced the van der Waals interaction, using the semiempirical Grimme's DFT-D2 method [27,28], to accurately obtain the geometry optimization of the models [29]. The kinetic energy cutoff for the wave functions and charge density were taken to be 0.408 keV and 8.163 keV, respectively. The Brillouin zone of the supercell was sampled by $9 \times 9 \times 1$ Monkhorst-Pack *k*-point grid. The XCrySDen package [30] was adopted to visualize and plot the structural models. After the geometry optimization, the band structure and the total and projected densities of states (PDOS) were calculated for each model using the Quantum Espresso package. Thereafter, the electrical conductivity and the electronic thermal conductivity were computed as a function of the chemical potential using the BoltzWann package [31].

The three structural models investigated in this work consist of a graphene supercell with eight atoms on a α-Al_2O_3 (0001) substrate, as shown in Fig. 1. The alumina surfaces terminate with Al atom (a and b) or O atom (c). In (a), the center of graphene hexagon is positioned over the Al atom Al_1, in (b) a C atom of graphene layer is on the top of the Al atom Al_2, and in (c) three C atoms are bonding to the topmost layer of oxygen. The α-Al_2O_3 (0001) slab, with approximately 18 *Å* thick, contains 12 (11) atoms of Al for slab terminating with Al (O) and 18 atoms of O in both the cases. A vacuum of approximately 18 *Å* was introduced in order to prevent any interaction between the layers. The thickness of the slabs vary between 11.08 and 11.94 Å.

The geometry optimization of Gr on the α-Al_2O_3 (0001) surface was carried out using two procedures:

i All atoms of the supercell were allowed to move in accordance with the BFGS quasi-Newton algorithm;
ii The atoms of the three topmost layers of the α-Al_2O_3 (0001) slab, including the C atoms, were allowed to move, whereas the atoms of the remaining slab layers were frozen in their respective atomic bulk positions.

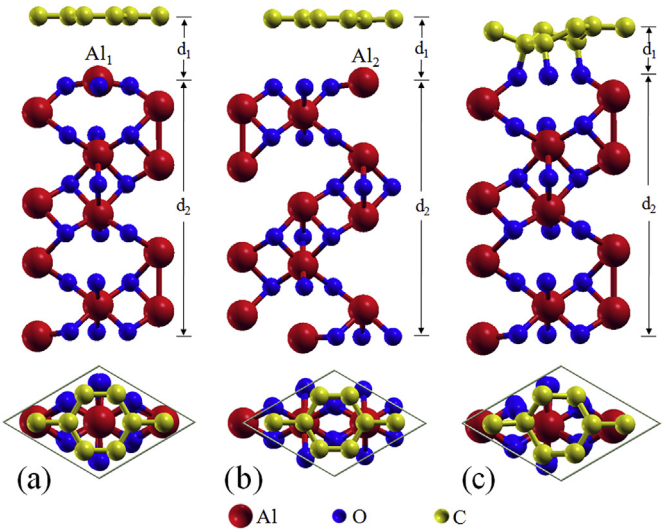

Fig. 1. Structural models for Gr on α-Al_2O_3 (0001) surface. In (a) and (b) the unit cell alumina surface terminates with one Al atom, with the Gr hexagonal center positioned above the Al_1 atom and a C atom over the Al_2 atom, respectively. In (c) the unit cell aluminasurface terminates with three O atoms, which are bonded to the three closer C atoms. The parameters d_1 and d_2 are presented in Table 1.

Maintaining the original bulk lattice parameter of 4.7605 Å, the supercell of Gr/α-Al_2O_3 (0001) was relaxed as follows: firstly, only the α-Al_2O_3 (0001) slab, obtained from the crystal bulk unit cell, was optimized. Then a Gr supercell with eight atoms was placed over the α-Al_2O_3 (0001) surface and a new optimization procedure was performed. For both surfaces terminating with Al or C atom, the lowest energy was obtained with the optimization procedure (**i**).

3. Results and discussion

The basic structural parameters of the models (a), (b) and (c) obtained from the geometry optimization procedures (**i**) and (**ii**) are shown in Table 1, where E_{coh} is the cohesion energy per atom in the unit cell, given in eV, d_0 is the distance between neighboring C atoms, d_1 is the distance between the bottom of the Gr layer and the α-Al_2O_3 (0001) surface and d_2 is the thickness of the slab. All the above distances are given in Angstrom.

The cohesion energy E_{coh} per atom in the unit cell is obtained from

Table 1
The model, geometry optimization process (Opt.) and their respective cohesion energy per atom in the unit cell (E_{coh}) (eV), distance d_0 (Å) between neighbors C atoms, distance d_1 (Å) between the bottom of the Gr layer and the α-Al_2O_3 (0001) surface, and the thickness d_2 (Å) of the slab.

Model	Opt.	E_{coh}	d_0	d_1	d_2
a) 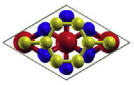	i	−7.36	1.38	2.91	11.36
	ii	−7.30	1.37	2.94	11.90
b) 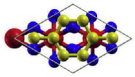	i	−7.36	1.37	2.76	11.35
	ii	−7.30	1.37	2.79	11.94
c) 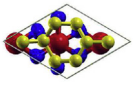	i	−7.20	1.36 to 1.54	1.43	11.08
	ii	−7.14		1.35	11.66

$$E_{coh} = \frac{E_{cell} - N_C E(C) - N_{Al} E(Al) - N_O E(O)}{N_A}, \quad (1)$$

where N_A is the total number of atoms per Gr/α-Al_2O_3 (0001) unit cell, which contains N_C atoms of C, N_{Al} atoms of Al and N_O atoms of O. E_{cell} is the total energy of the cell and E(C), E(Al) and E(O) are the energies corresponding to each isolated atom of C, Al and O, respectively. It is observed that the configurations (a, **i**) and (b, **i**) present the lowest cohesion energy. In models (a) and (b) the bonding length between nearest neighbors in Gr varies from 1.37 to 1.38 *Å*, which represents a mismatch of approximately 3% in relation to the pristine Gr. For models whose surface terminates with Al atoms, the interplanar distances d_1 is smaller for model (b). In all of the models the slab thickness d_2 is smaller than that of 12.51 *Å* of the bulk crystal unit cell. In model (c), where the Gr layer is placed on the top of the α-Al_2O_3 (0001) slab terminating with O atom, there is a strong decrease in the O–C bonding, due to the charge transfer from carbon to oxygen, whereas the C–C bonding lengths vary between 1.36 and 1.54 *Å*, with the C atoms distributed in two planes separated by 0.635 *Å*.

The results for the band structures and transport properties of each model will be presented separately based on the geometry optimization processes (**i**) and (**ii**). The band structures and the projected density of states (PDOS) of the individual atoms are shown in Fig. 2 for the configurations belonging to the optimization process (**i**). At the left-hand column we present the band structures whereas the corresponding PDOS are on the right-hand side. In (a, **i**), the band structure of the pristine Gr is introduced into the gap of the α-Al_2O_3 (0001). The conduction and the valence π bands (CB and VB, respectively) are similar to the π bands of pristine Gr around the Dirac K symmetry point. The similarity between the density of states of the pristine Gr (light blue) and the PDOS of Gr/α-Al_2O_3 (0001) (red) can be seen from the PDOS spectrum. There is practically no contribution of the Al and O atoms to the PDOS of VB and CB. Moreover, analyzing the results presented in Fig. 2, we observe that the valence and conduction π bands of (b, **i**) are apparently similar to the case (a, **i**). In Fig. 2 (c) the surface terminates with O atoms with a large charge transfer between carbon and oxygen atoms, opening an indirect gap of 1.19 eV between the two π bands of Gr. The lower band becomes the conduction band formed by π orbitals of three carbon atoms of the sublattice A and three oxygen atoms of the α-Al_2O_3 (0001) surface which are directly bound to the carbon atoms.

In Fig. 3, the PDOS is described in terms of the contributions of the *s* and *p* orbitals. In Fig. 3(a) for model (a, **i**), there is a good consonance between the *p* orbital PDOS (red color) and the density of states of pristine Gr (blue color) close to the Fermi level. However, PDOS for model (b, **i**) differs from that of model (a, **i**) and also from that of pristine graphene. In this case, the similarity between the PDOS of Gr/α-Al_2O_3 (0001) and the pristine Gr around the Fermi level occurs mainly for energy above ε_F. Fig. 3 (c) exhibits a strong contribution of the π orbitals to the density of states of Gr/α-Al_2O_3 around the Fermi level.

From Table 2, for case (a, **i**), we can see that the valence and conduction π bands are formed essentially from $2p_z$ orbitals of the carbon atoms. Using the notation A and B to label the two triangular Gr sub-lattices [32,33], each one with a basis of two atoms per unit cell, there are four Gr unit cells on the α-Al_2O_3 (0001) surface,

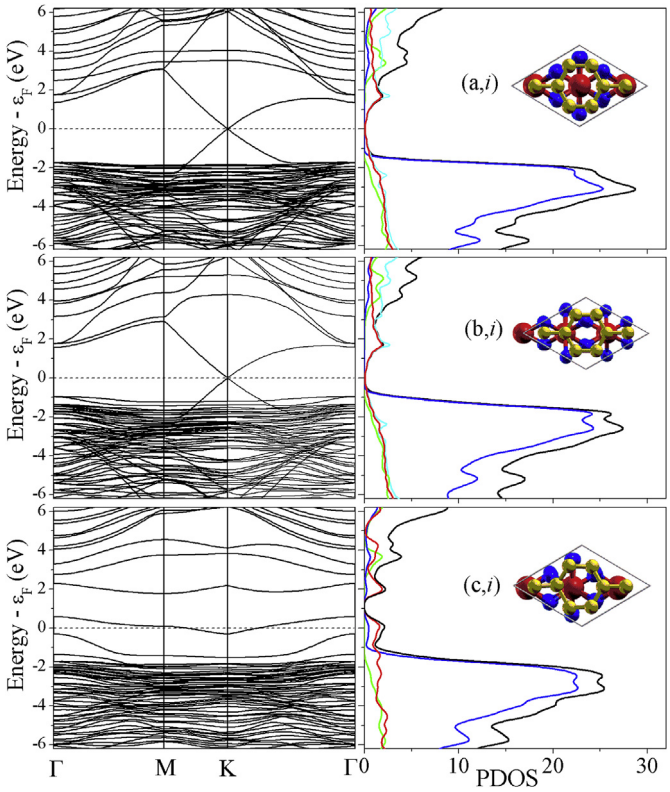

Fig. 2. Band structure (left) and projected density of states (PDOS) (right) of the models for Gr on α-Al_2O_3 (0001) surface (a, **i**), (b, **i**) and (c, **i**). The PDOS spectra are for C (red), O (blue), Al (green), total PDOS (black) (sum of the contribution of C, O and Al) and pristine Gr (light blue). (For interpretation of the references to colour in this figure legend, the reader is referred to the web version of this article.)

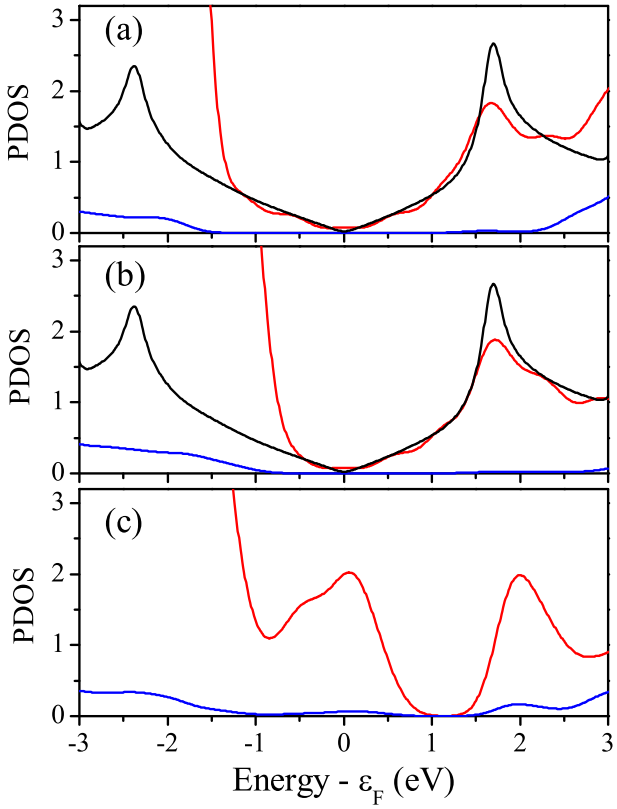

Fig. 3. Projected density of states (PDOS) of p (red) and s (blue) orbitals for Gr on α-Al_2O_3 (0001) surface, compared with the PDOS of pristine Gr (black). (a), (b) and (c) correspond to the models presented in Table 1 and Fig. 2. (For interpretation of the references to colour in this figure legend, the reader is referred to the web version of this article.)

Table 2
Contributions of the atomic orbital to the valence and conduction band of Gr/α-Al_2O_3 (0001) for the model (a, **i**).

Valence Band			Conduction Band		
C atom	Orbital	$\|\Psi\|^2$	C atom	Orbital	$\|\Psi\|^2$
A_1	$2p_z$	0.248	A_1	$2p_z$	0.004
A_2	$2p_z$	0.242	A_2	$2p_z$	0.004
A_3	$2p_z$	0.241	A_3	$2p_z$	0.003
A_4	$2p_z$	0.241	A_4	$2p_z$	0.004
B_1	$2p_z$	0.004	B_1	$2p_z$	0.247
B_2	$2p_z$	0.004	B_2	$2p_z$	0.241
B_3	$2p_z$	0.004	B_3	$2p_z$	0.241
B_4	$2p_z$	0.003	B_4	$2p_z$	0.241
O	$2p_z$	–	O	$2p_z$	0.001

whose atoms are labelled in Table 2 as A_i and B_i, $i = 1, 2, 3, 4$. The valence band is composed practically of $2p_z$ carbon orbitals from the sublattice *A*, whereas the conduction band is formed of p_z carbon of sublattice *B*.

From Table 3, for case (b, **i**), the valence and the conduction π bands are formed significantly by the $2p_z$ carbon orbitals of the Gr sublattices A and B, respectively, but there is also a small contribution from the $2p_z$ orbital of the Al atoms.

In Fig. 4 (a) the electrical conductivity and (b) the electronic thermal conductivity divided by the relaxation time of Gr (black color) are demonstrated for the three models described in Table 1 as (a, **i**), (b, **i**) and (c, **i**). For the models (a, **i**) (red color) and (b, **i**) (blue color) both the electrical and thermal electronic conductivities present the linear behavior as that of Gr (black color). For both the above cases, the values of the transport properties of Gr/α-Al_2O_3 (0001) slab are lower than that of pristine Gr, due to the mismatch of 3% between the lattices of Gr and α-Al_2O_3 (0001), which increases the electronic scattering of the conduction electrons. On the other hand, the model (c, **i**) lost that linear characteristic. The O atoms of the α-Al_2O_3 (0001) surface interact differently with the C atoms of sublattice A and B of Gr. For each unit cell of Gr/α-Al_2O_3 (0001) slab, two oxygen atoms interact with two C atoms of sublattice A and only one O atom interacts with one C atom of superlattice B. This breaks the equivalence between the two Gr sublattice and destroys the electronic peculiar behavior around the Dirac symmetry K point.

Let us now consider the cases pertaining to the geometry optimization process (**ii**). The band structure and the projected density of states are shown in Fig. 5. The π valence and conduction bands of Gr appear inside the band gap of the α-Al_2O_3 (0001) slab for (a, **ii**) and (b, **ii**), as also observed for (a, **i**) and (b, **i**). However, there is a mini-gap in the band structures of (a, **ii**) and (b, **ii**) of 35 meV and

Table 3
Contributions of the atomic orbital to the valence and conduction band of Gr/α-Al_2O_3 (0001) for the model (b, **i**).

Valence Band			Conduction Band		
C atom	Orbital	$\|\Psi\|^2$	C atom	Orbital	$\|\Psi\|^2$
A_1	$2p_z$	0.246	A_1	$2p_z$	–
A_2	$2p_z$	0.246	A_2	$2p_z$	–
A_3	$2p_z$	0.224	A_3	$2p_z$	–
A_4	$2p_z$	0.246	A_4	$2p_z$	–
B_1	$2p_z$	0.002	B_1	$2p_z$	0.245
B_2	$2p_z$	0.001	B_2	$2p_z$	0.246
B_3	$2p_z$	–	B_3	$2p_z$	0.248
B_4	$2p_z$	–	B_4	$2p_z$	0.246
Al	$2p_z$	0.014	Al	$2p_z$	–
Al	$1s$	0.004	Al	$2p_z$	–
O	$2p_x$	0.001	O	$2p_z$	–

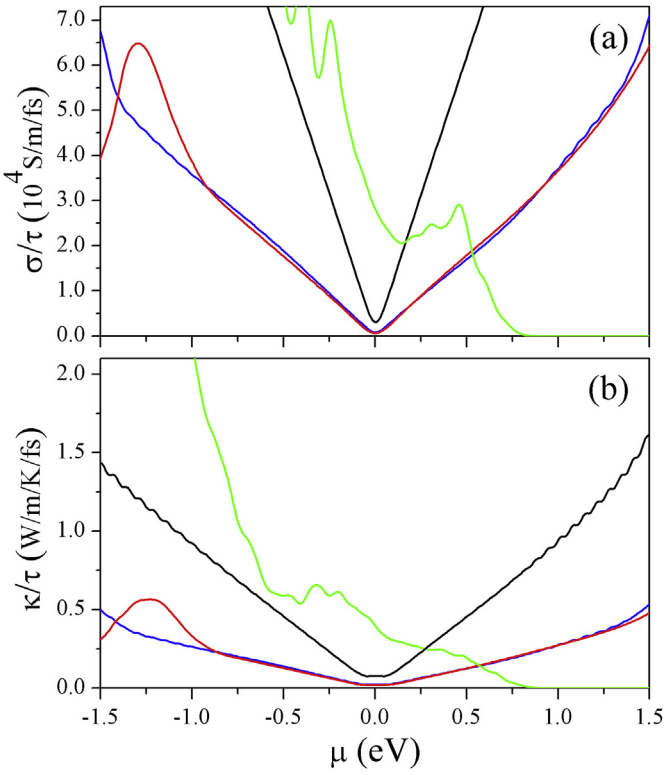

Fig. 4. Electrical conductivity (a) and electronic thermal conductivity (b) divided by the relaxation time τ as a function of the chemical potential μ for (a, **i**) (red color), (b, **i**) (blue color) and (c, **i**) (light green color). For the sake of comparison, the conductivity of pristine Gr is also presented (black color). (For interpretation of the references to colour in this figure legend, the reader is referred to the web version of this article.)

70 meV, respectively. In (a, **ii**) the Fermi level is 85 meV below the energy of the K Dirac symmetry point, revealing a p-type semiconducting behavior, while in (b, **ii**) this gap is less pronounced. In (b, **ii**) the Fermi level is immediately below the top of the valence band. In both cases, two *sp* bands are introduced, crossing with the two Gr bands. These new bands are formed from the *s* and *p* orbitals of Al and O atoms localized in the bottom of the α-Al_2O_3 (0001) slab. In (c, **ii**) the charge transfer between C and O atoms splits the π Gr bands, creating an indirect gap of 1.2 eV between the M and the Γ symmetry points.

Fig. 6 exhibits (a) the electrical conductivity and (b) the electronic thermal conductivity for the cases (a, **ii**) (red color), (b, **ii**) (blue color) and (c, **ii**) (light green color). For (a, **ii**) and (b, **ii**) we observe that the conductivity is approximately linear very close to the minimum. Moreover, the minima (a, **ii**) and (b, **ii**) are dislocated to the right of that of pristine Gr. Thus the above behavior corroborates the p-type semiconducting characteristic. The conductivity of the case (c, **ii**) is qualitatively different from Gr because of the breakdown of the electronic structure of Gr due to the charge transfer between the C and O atoms. The thermal conductivity for models (a, **ii**) and (b, **ii**) are less than that of pristine Gr and the qualitative behavior are very similar to that of (a, **i**) and (b, **i**). However κ/τ for (c, **ii**) differs significantly from that of (c, **i**). Unlike κ/τ, σ/τ suffers little change due to the optimization procedure.

In Tables 4 and 6 the contributions from the sublattices A and B of Gr atoms band structures are presented for the models (a, **ii**) and (b, **ii**), respectively. The valence bands are formed essentially by the sublattice A orbitals and the conduction bands by the sublattice B orbitals. Tables 5 and 7 exhibits the contributions of Al and O atoms for the *sp* bands of the models (a,**ii**) and (b, **ii**), respectively, which

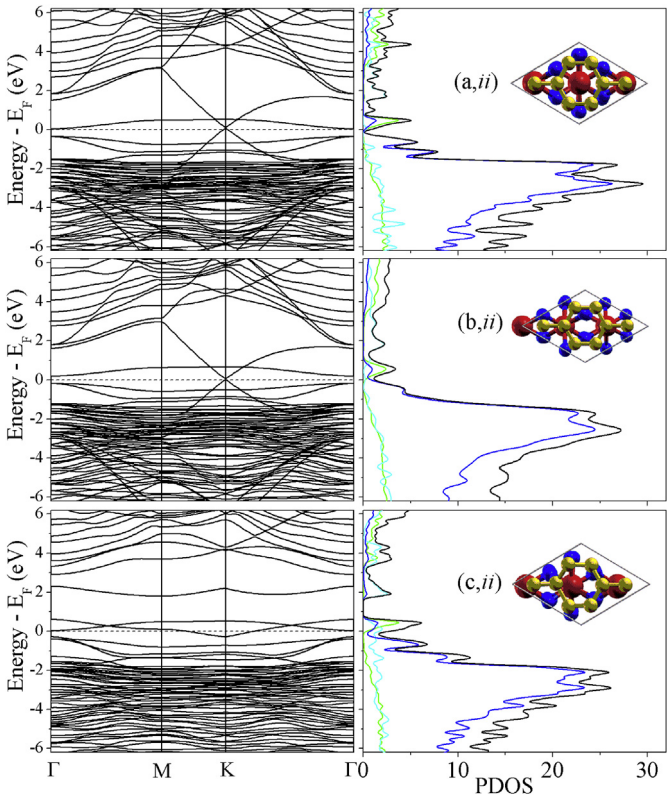

Fig. 5. Bands structure (left) and projected density of states (PDOS) (right) of the models for Gr on α-Al_2O_3 (0001) surface for the models (a, **ii**), (b, **ii**) and (c, **ii**), correspond to the configurations described in Table 1. The PDOS spectra are for C (red), O (blue), Al (green), total PDOS (black) (sum of the contribution of C, O and Al) and pristine Gr (light blue). (For interpretation of the references to colour in this figure legend, the reader is referred to the web version of this article.)

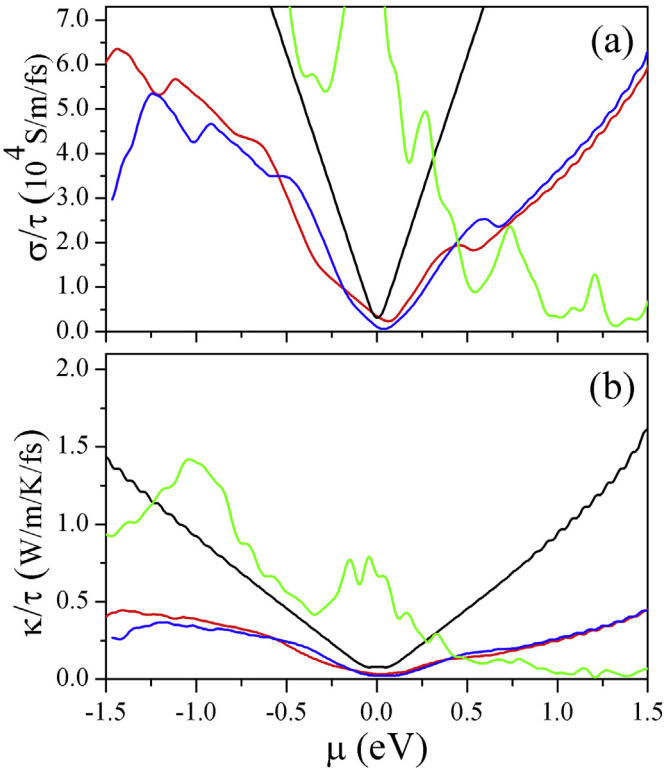

Fig. 6. Electrical conductivity (a) and electronic thermal conductivity (b) divided by the relaxation time τ as a function of the chemical potential μ for (a, **ii**) (red color), (b, **ii**) (blue color) and (c, **ii**) (light green color). For the sake of comparison, the conductivity of pristine Gr is also presented (black color). (For interpretation of the references to colour in this figure legend, the reader is referred to the web version of this article.)

crosses the valence and conduction bands. The contributions of the Al and O atoms dominate in the upper and the lower bands, respectively.

4. Conclusion

We studied the electronic structure and transport properties of a single layer of graphene (Gr) on α-Al_2O_3 surface using density functional theory (DFT). We analyzed six cases classified on the basis of the geometric optimization process and the types of atoms with which the alumina surfaces terminate. The band structure, the projected density of states, the electrical and the thermal electronic conductivities were calculated. The calculations revealed the following results: 1) the models (a, **i**) and (b, **i**) that terminate with Al atoms and the optimization allowed all atoms of the supercell to move in accordance with the BFGS quasi-Newton algorithm preserve qualitatively the band structures and the electrical and thermal electronic properties of the pristine Gr. However, in both the cases, the conductivities are smaller than that of pristine Gr due to the mismatch of the lattice parameters of Gr and the α-Al_2O_3 (0001) slab. 2) the above models which allowed the three topmost layers of the α-Al_2O_3 (0001) slab, including the C atoms, to move, whereas the atoms of the remaining layers were frozen in their atomic bulk positions (a, **ii**) and (b, **ii**) present a mini-gap at the Dirac symmetry point, with the Fermi level below and above the conduction band for models (a, **ii**) and (b, **ii**), respectively. 3) The models where the surface terminated with oxygen atoms (c, **i**) and (c, **ii**) irrespective of the optimization procedure lost the

Table 4
Contributions of the atomic orbital to the valence and conduction band of Gr/α-Al_2O_3 (0001) for the model (a, **ii**).

Valence Band			Conduction Band		
C atom	Orbital	$\lvert\Psi\rvert^2$	C atom	Orbital	$\lvert\Psi\rvert^2$
A_1	$2p_z$	0.250	A_1	$2p_z$	0.001
A_2	$2p_z$	0.243	A_2	$2p_z$	0.002
A_3	$2p_z$	0.243	A_3	$2p_z$	–
A_4	$2p_z$	0.243	A_4	$2p_z$	0.001
B_1	$2p_z$	0.001	B_1	$2p_z$	0.249
B_2	$2p_z$	0.001	B_2	$2p_z$	0.243
B_3	$2p_z$	0.002	B_3	$2p_z$	0.243
B_4	$2p_z$	–	B_4	$2p_z$	0.243
O	$2p_z$	–	O	$2p_z$	0.001

Table 5
Contributions of the Al and O atomic orbital to the energy bands inside the gap of the α-Al_2O_3 (0001) slab for the model (a, **ii**).

Atom	lower band		Upper band	
	Orbital	$\lvert\Psi\rvert^2$	Orbital	$\lvert\Psi\rvert^2$
O	$2s$	0.003	$1s$	0.012
	$2p_x$	0.059	$2p_x$	0.009
	$2p_y$	0.697	$2p_y$	0.011
	$2p_z$	0.212	$2p_z$	0.198
Al	$2s$	0.002	$1s$	0.275
	$2p_x$	–	$2p_x$	0.017
	$2p_y$	–	$2p_y$	0.009
	$2p_z$	0.002	$2p_z$	0.424

Table 6
Contributions of the atomic orbital to the valence and conduction band of Gr/α-Al_2O_3 (0001) for the model (b, **ii**).

Valence Band			Conduction Band		
C atom	Orbital	$\|\Psi\|^2$	C atom	Orbital	$\|\Psi\|^2$
A_1	$2p_z$	0.248	A_1	$2p_z$	0.002
A_2	$2p_z$	0.248	A_2	$2p_z$	0.001
A_3	$2p_z$	0.247	A_3	$2p_z$	0.001
A_4	$2p_z$	0.244	A_4	$2p_z$	0.001
B_1	$2p_z$	0.002	B_1	$2p_z$	0.247
B_2	$2p_z$	0.001	B_2	$2p_z$	0.246
B_3	$2p_z$	0.001	B_3	$2p_z$	0.248
B_4	$2p_z$	0.001	B_4	$2p_z$	0.247
Al	$2p_z$	–	O	$2p_z$	0.001

Table 7
Contributions of the Al and O atomic orbital to the energy bands inside the gap of the α-Al_2O_3 (0001) slab for the model (b, **ii**).

Atom	lower band		Upper band	
	Orbital	$\|\Psi\|^2$	Orbital	$\|\Psi\|^2$
O	1*s*	0.003	1*s*	–
	$2p_x$	0.351	$2p_x$	0.080
	$2p_y$	0.361	$2p_y$	0.020
	$2p_z$	0.254	$2p_z$	0.145
Al	2*s*	0.002	2*s*	0.278
	$2p_x$	–	$2p_x$	0.017
	$2p_y$	–	$2p_y$	0.017
	$2p_z$	0.002	$2p_z$	0.425

characteristic electronic structure of pristine Gr due to a significant charge transfer between the carbon and oxygen atoms on the substrate surface.

Financial support

The authors acknowledge financial support from the Brazilian funding agency CNPq.

References

[1] K.S. Novoselov, A.K. Geim, S.V. Morozov, D. Jiang, Y. Zhang, S.V. Dubonos, I.V. Grigorieva, A.A. Firsov, Science 306 (2004) 666.
[2] K.S. Novoselov, et al., Nat. Lond. 438 (2005) 197.
[3] A.K. Geim, K.S. Novoselov, et al., Nat. Mater 6 (2007) 183.
[4] C.N.R. Rao, K. Biswas, K.S. Subrahmanyam, A. Govindaraj, J. Mater. Chem. 19 (2009) 2457.
[5] S. Guo, S. Dong, Chem. Soc. Rev. 40 (2011) 2644.
[6] I.A. Brytov, Yu. N. Romashchenko, Fiz. Tverd. Tela Leningr. 20 (1978) 664 [Sov. Phys. Solid State 20, 384(1978)].
[7] Y.-N. Xu, W.Y. Ching, Phys. Rev. B 43 (1991) 4461.
[8] K. Shiiki, M. Igorashi, H. Kaijyu, Jpn. J. Appl. Phys. Part 1 (42) (2003) 5185.
[9] J. Robertson, J. Appl. Phys. 92 (2002) 4712.
[10] J. Robertson, Eur. Phys. J. Appl. Phys. 28 (2004) 265.
[11] T.V. Perevalov, A.V. Shaposhnikov, V.A. Gritsenko, H. Wong, J.H. Han, C.W. Kim, JETP Lett. 85 (2007) 165.
[12] M.I. Boltz, R.H. French, Appl. Phys. Lett. 55 (1989) 1955.
[13] S. Kim, J. Nah, I. Jo, D. Shahrjerdi, L. Colombo, Z. Yao, E. Tutuc, S.K. Banerjee, Appl. Phys. Lett. 94 (2009) 062107.
[14] L. Liao, J. Bai, Y. Qu, Y. Huang, X. Duan, Nanotechnology 21 (2010) 015705.
[15] L. Han, S. Qing-Qing, C. Lin, X. Yan, D. Shi-Jin, Z. Wei, Z. Shi-Li, Chin. Phys. Lett. 27 (2010) 077201.
[16] P. Jadaun, S.K. Banerjee, L.F. Register, B. Sahu, J. Phys. Condens. Matter 23 (2011) 505503.
[17] B. Huang, Q. Xu, S.-H. Wei, Phys. Rev. B 84 (2011) 155406.
[18] V.V. Ilyasov, I.V. Ershov, Phys. Solid State 54 (2012) 2335.
[19] P. Jadaun, B.R. Sahu, L.F. Register, S.K. Banerjee, Solid State Commun. 152 (2012) 1497.
[20] L. Omiciuolo, E.R. Hernndez, E. Miniussi, F. Orlando, P. Lacovig, S. Lizzit, T.O. Mentes, A. Locatelli, R. Larciprete, M. Bianchi, S. Ulstrup, P. Hofmann, D. Alf, A. Baraldi, Nat. Commun. 5 (2014) 5062.
[21] V.V. Ilyasov, I.V. Ershov, A.V. Ilyasov, I.G. Popova, C.V. Nguyen, Surf. Sci. 632 (2015) 111.
[22] J.M. Polfus, O.M. Lvvik, P.M. Rrvik, R. Bredesen, J. Eur. Ceram. Soc. 36 (2016) 719.
[23] P. Giannozzi, et al., J. Phys. Condens. Matter 21 (2009) 1–19.
[24] G. Pizzia, D. Voljab, B. Kozinskyc, M. Fornari, N. Marzaria, Comput. Phys. Commun. 185 (2014) 422.
[25] P. Giannozzi, et al., J. Phys. Condens. Matter 21 (2009) 1–19.
[26] M.C. Payne, M.P. Teter, C. Allan, T.A. Arias, J.D. Joannopoulos, Rev. Mod. Phys. 64 (1992) 1045, https://doi.org/10.1103/RevModPhys.64.1045.
[27] S. Grimme, J. Comput. Chem. 27 (2006) 1787.
[28] V. Barone, M. Casarin, D. Forrer, M. Pavone, M. Sambi, A. Vittadini, J. Comp. Chem. 30 (2009) 934.
[29] G. Mercurio, E.R. McNellis, I. Martin, S. Hagen, F. Leyssner, S. Soubatch, J. Meyer, M. Wolf, P. Tegeder, F.S. Tautz, K. Reuter, Phys. Rev. Lett. 104 (2010) 036102.
[30] A. Kokalj, Comput. Mater. Sci. 28 (2003) 155, https://doi.org/10.1016/S0927-0256(03)00104-6.
[31] G. Pizzia, D. Voljab, B. Kozinskyc, M. Fornari, N. Marzaria, Comput. Phys. Commun. 185 (2014) 422.
[32] A.H. Castro Neto, F. Guinea, N.M.R. Peres, K.S. Novoselov, A.K. Geim, Rev. Mod. Phys. 81 (2009) 109.
[33] S. Das Sarma, Shaffique Adam, E.H. Hwang, Enrico Rossi, Rev. Mod. Phys. 83 (2011) 407.